SUPPLEMENTARY INFORMATION

Tailored Hybridization of MIL-101(Cr) with Graphene Oxide Enables Enhanced Hydrogen Storage and Delivery

Laura Jimenez Lopez [a], Rosana V. Pinto [c], Rafael Morales Ospino [a], Jimena Castro-Gutierrez [a], Farid Nouar [c], Georges Mouchaham [c], Alain Celzard [a,b], Christian Serre [c], Vanessa Fierro [a,*]

[a] *Université de Lorraine, CNRS, IJL, F-88000, Epinal, France;*

[b] *Institut Universitaire de France (IUF), 75231, Paris, France*

[c] *Institut des Matériaux Poreux de Paris, Ecole Normale Supérieure, ESPCI Paris, CNRS, PSL University, 75005 Paris, France*

*** Corresponding author.** Tel: + 33 372 74 96 77.

Fax: + 33 372 74 96 38.

E-mail address: Vanessa.Fierro@univ-lorraine.fr (V. Fierro)

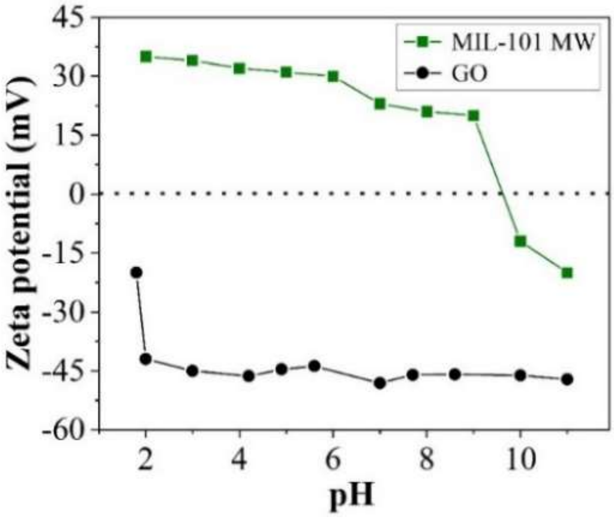

Figure S1: Zeta potential as a function of pH for pure GO and pure MIL-101(Cr).

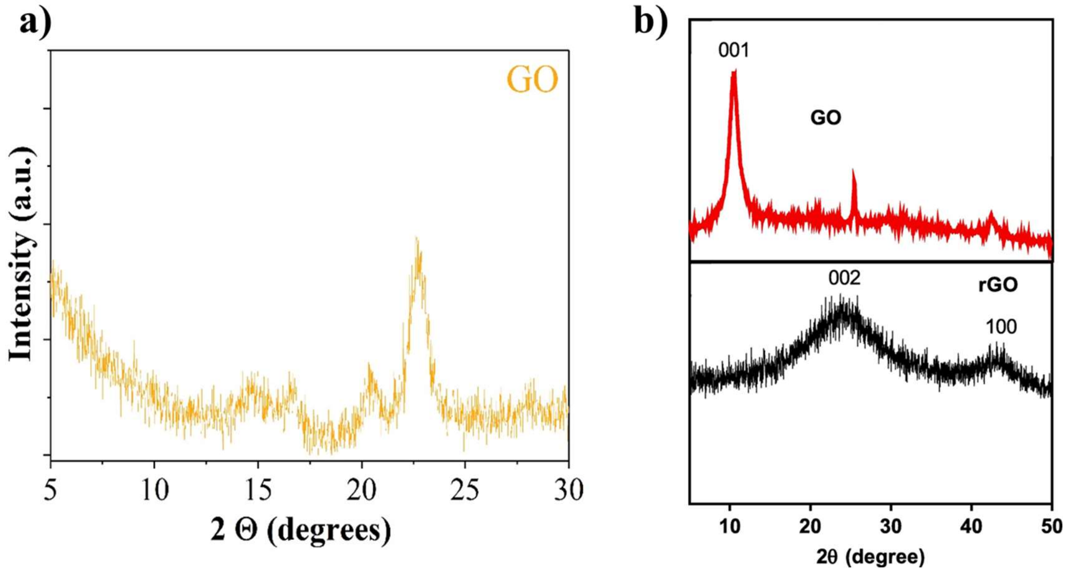

Figure S.2: X-ray diffraction patterns (Cu Kα, 1.5406 Å) of the commercial GO used in this study; b) XRD comparison of GO and rGO reported in Ref. [1].

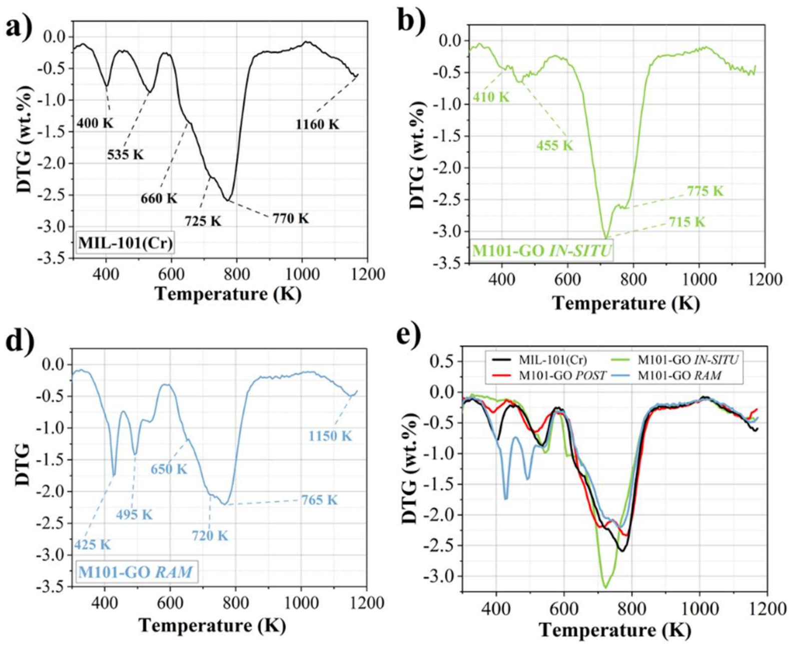

Figure S3: DTG of: a) MIL-101(Cr) synthesized by microwave-assisted method; b) M101-GO *IN-SITU* (hybrid containing 5 wt.% GO synthesized by *in-situ* method); c) M101-GO *POST* (hybrid containing 5 wt.% GO synthesized by post hybridization); d) M101-GO RAM (hybrid containing 5 wt.% GO synthesized by RAM); e) Comparison of all samples.

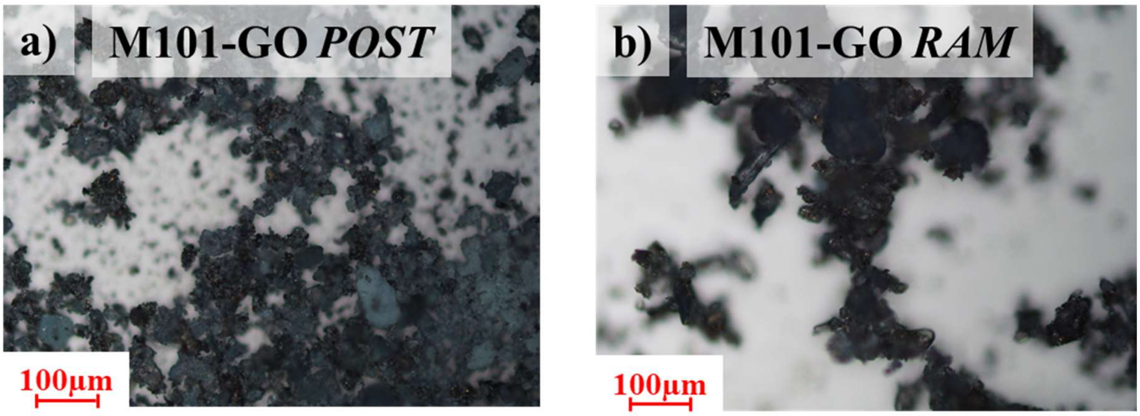

Figure S4: Optical microscopy images: a) M101-GO IN-SITU; b) M101-GO POST; and e) M101-GO RAM.

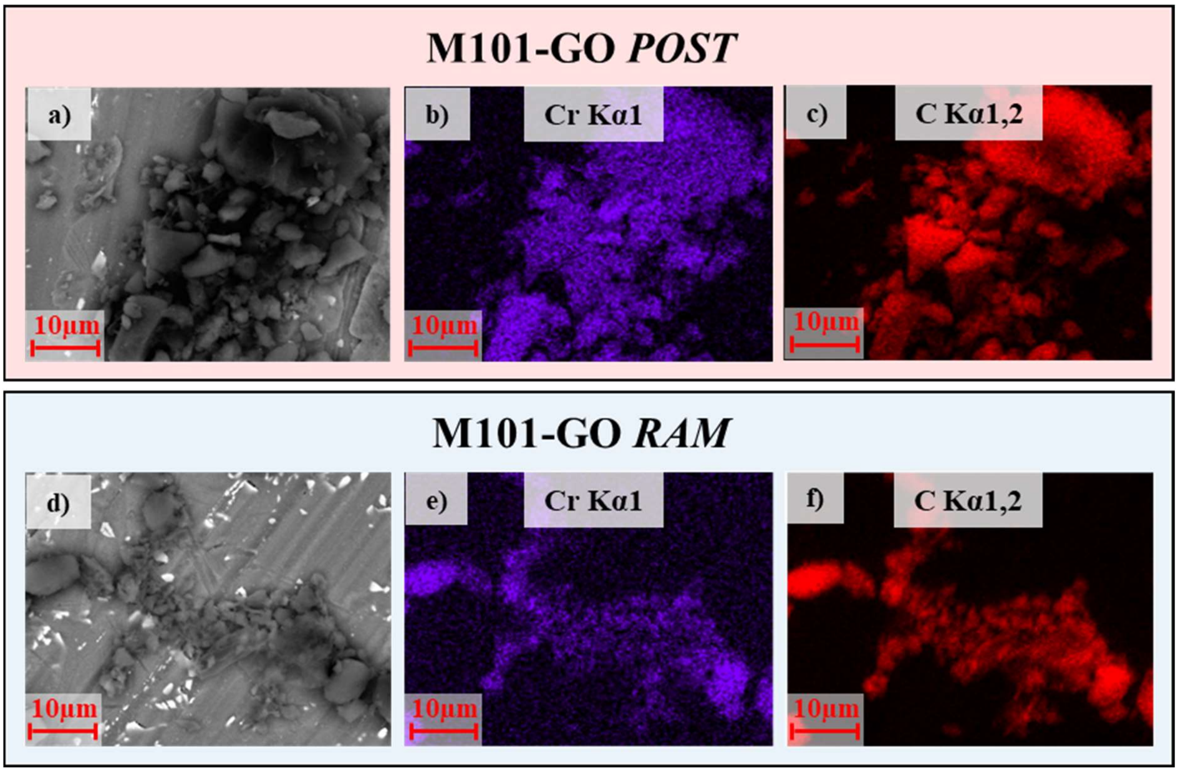

Figure S5: a) SEM image of M101-GO *POST*, with its corresponding b) chromium and c) carbon elemental maps; and d) SEM image of M101-GO *RAM* , with its corresponding e) chromium and f) carbon elemental maps.

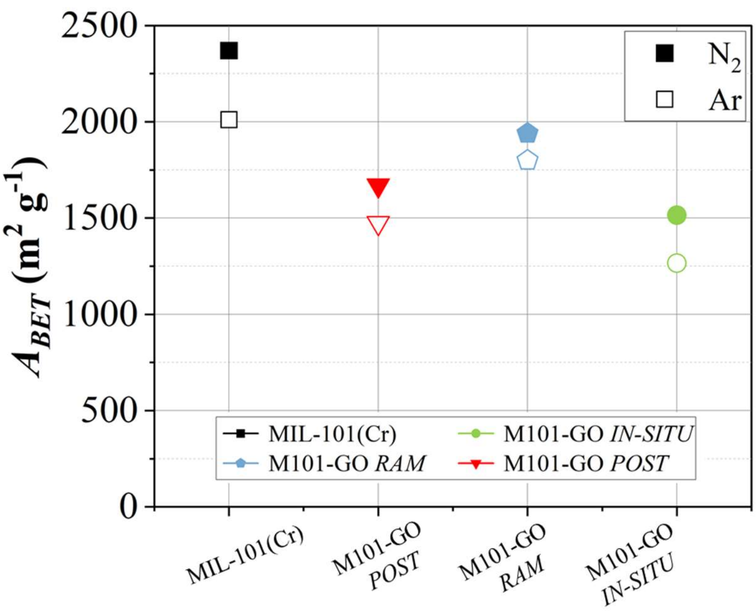

Figure S6: Comparative of BET areas obtained from either N_2 or Ar isotherms.

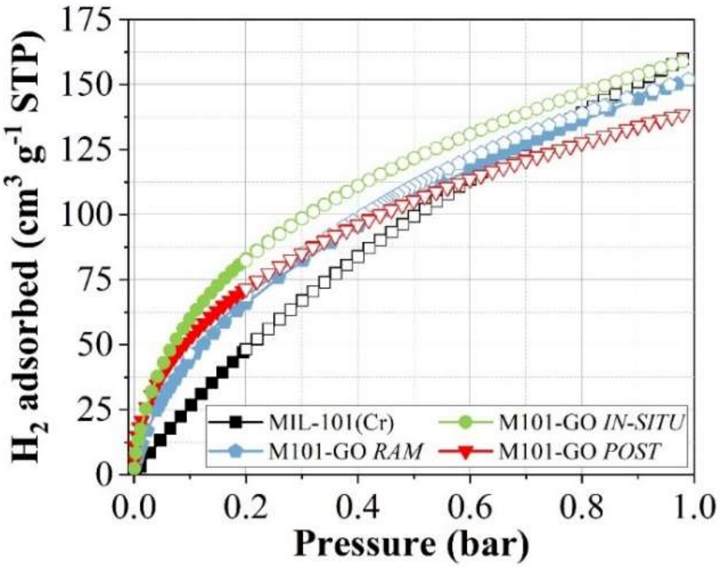

Figure S7: H_2 adsorption (full symbols)-desorption (empty symbols) isotherms at 77 K of pure MIL-101(Cr) and hybrids.

Table S1: Textural properties of pure HKUST-1 and hybrid materials prepared in this study.

Method	*Parameter*	MIL-101(Cr)	M101-GO *POST*	M101-GO *RAM*	M101-GO *IN SITU*
BET at 77K	$A_{BET\ N2}$ ($m^2\ g^{-1}$)	2370	1670	1940	1515
	$A_{BET\ Ar}$ ($m^2\ g^{-1}$)	2010	1475	1800	1265
V_T at p/p°=0.97	$V_{T\ N2}$ ($cm^3\ g^{-1}$)	2.44	1.28	2.03	0.85
	$V_{T\ AR}$ ($cm^3\ g^{-1}$)	2.12	1.14	1.98	0.75
2D-NLDFT N_2 and H_2 at 77 K	$S_{2D\text{-}NLDFT}$ ($m^2\ g^{-1}$)	1465	1180	1280	1158
	$V_{T2D\text{-}NLDFT}$ ($cm^3\ g^{-1}$)	2.23	1.20	1.91	0.79
	V_{meso} ($cm^3\ g^{-1}$)	1.54	0.65	1.34	0.29
	V_{micro} ($cm^3\ g^{-1}$)	0.69	0.55	0.57	0.50
	V_{sm} ($cm^3\ g^{-1}$)	0.69	0.50	0.53	0.35
	$V_{\mu m}$ ($cm^3\ g^{-1}$)	0.00	0.05	0.04	0.15
Density	ρ_{tap} ($kg\ m^{-3}$)	259	290	295	426
	ρ_{skel} ($kg\ m^{-3}$)	2450	1892	1876	1794

The surface area, A_{BET}, was determined using the BET equation applied to the adsorption isotherms of nitrogen and argon. Total pore volumes, V_{TN2} and V_{TAr}, were calculated from N_2 and Ar isotherms at p/p°=0.97. The 2D-NLDFT-HS model was applied to N_2 and H_2 adsorption data at 77 K.

Table S2: Excess H_2 uptake (wt.%), total H_2 uptake (wt.%), total H_2 uptake (kg m^{-3}) and release capacity (kg m^{-3}) for the pure MOF and hybrid materials.

Quantity	***Conditions***	**MIL-101(Cr)**	**M101-GO *POST***	**M101-GO *RAM***	**M101-GO *IN SITU***
n_{exc} (wt.%)	77K; 40 bars	3.8 ± 0.1	3.0 ± 0.1	3.2 ± 0.1	2.9 ± 0.1
	160K; 100 bars	2.5 ± 0.1	2.6 ± 0.1	2.7 ± 0.1	1.7 ± 0.1
	273K; 100 bars	0.6 ± 0.2	0.6 ± 0.0	0.7 ± 0.0	0.5 ± 0.0
n^{v}_{tot} (kg m^{-3})	77K; 100 bars	33.8 ± 1.0	33.6 ± 1.0	33.5 ± 1.0	36.0 ± 1.1
	77K; 5 bars	7.1 ± 0.2	7.0 ± 0.4	7.8 ± 0.2	9.4 ± 0.3
	160K; 5 bars	1.3± 0.0	1.1 ± 0.0	1.4 ± 0.04	1.5 ± 0.0
Release capacity (kg m^{-3})	$R^{77K\rightarrow77K}$	26.7 ± 0.8	26.7 ± 0.8	25.7 ± 0.8	26.6 ± 0.8
	$R^{77K\rightarrow160K}$	32.5 ± 1.0	34.1 ± 1.2	32.1 ± 1.0	34.5 ± 1.0

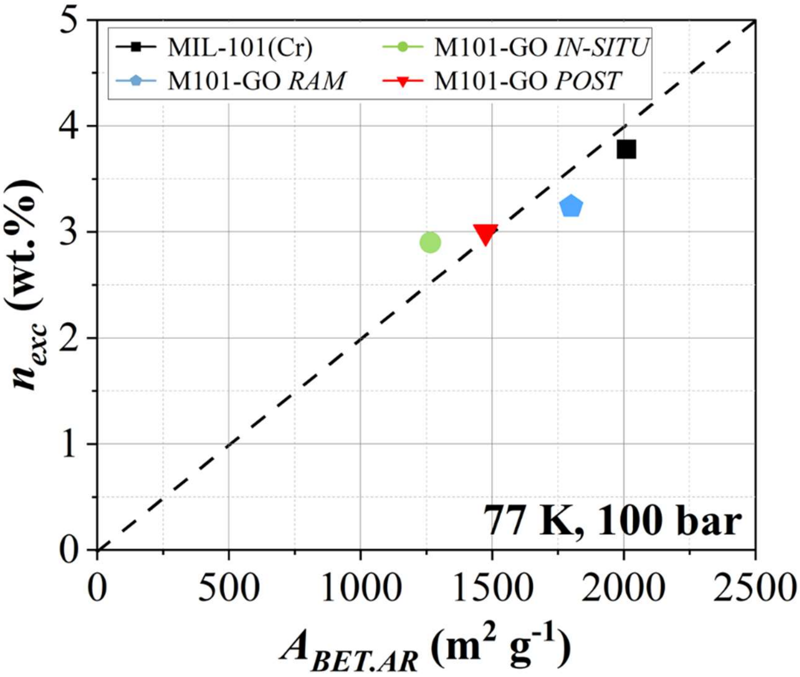

Figure S8: Chahine's rule (black, dashed line) of pure MIL-101(Cr) and hybrids as a function of their BET area calculated from argon adsorption data, $A_{BET.AR}$.

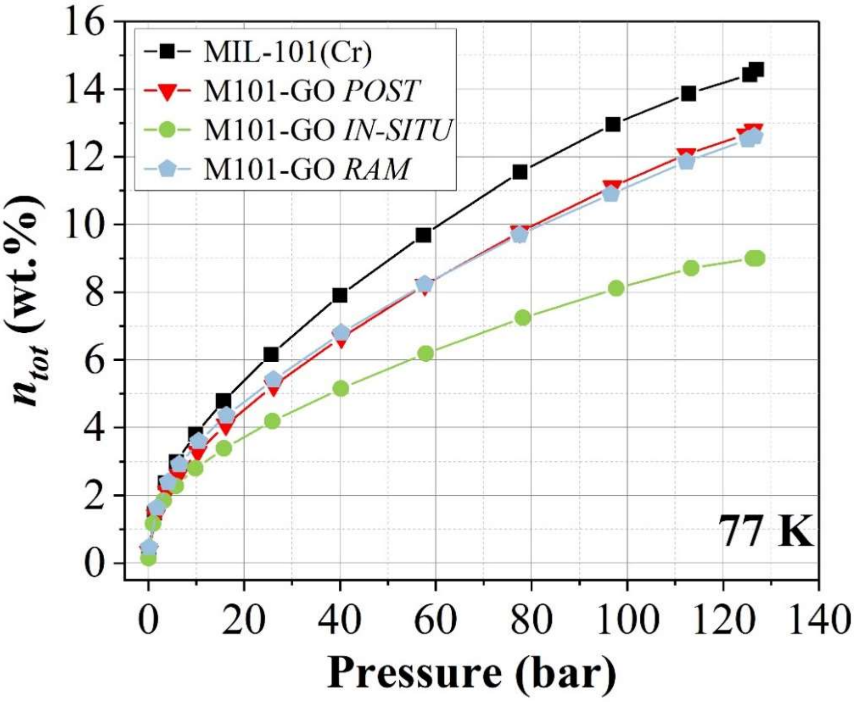

Figure S9: n_{tot} at 77 K (wt.%) of hybrids and pure MOF.

Table S3: Total H_2 stored (kg m^{-3}), release $^{77K\rightarrow160K}$ capacity and release $^{77K\rightarrow77K}$ capacity.

Sample	*Total stored* (kg m^{-3})	*Release $^{77K\rightarrow160K}$* (kg m^{-3})	% Release	*Release $^{77K\rightarrow77K}$* (kg m^{-3})	% Release
Empty tank	31.0	30.4	98	29.5	95
MIL-101(Cr*)*	33.8 ± 1.0	32.5 ± 1.0	96	26.7 ± 0.8	79
M101-GO *POST*	33.6 ± 1.0	34.1 ± 1.0	95	26.7 ± 0.8	79
M101-GO *RAM*	33.5 ± 1.0	32.1 ± 1.0	96	25.7 ± 0.8	77
M101-GO *IN-SITU*	36.0 ± 1.1	34.5 ± 1.0	96	26.6 ± 0.8	74

Table S 4: Excess hydrogen storage in gravimetric capacities (n_{exc}, wt.%) of selected MOFs reported in the literature under similar conditions (77 K, 20-60 bar).

Sample	Temperature (K)	Pression (Bar)	A_{BET} (m^2 g^{-1})	Excess H_2 uptake (wt.%)	Ref.
HKUST-1	77	42	1116	2.80	[2]
HKUST-1@GO	77	42	734	3.60	[2]
MIL-101(Cr)	77	60	2887	2.90	[3]
MIL-101(Cr) @SWCNT	77	60	2998	4.40	[3]
MIL-101	77	100	3223	3.90	[4]
MIL101@AC	77	51	3542	4.40	[4]
IRMOF-2	77	25	1700	2.50	[5]
MFU-4l	77	20	1670	2.50	[6]
MIL-100(Al)	77	40	1200	3.10	[7]
MIL-100(Al)@Pd	77	40	380	1.30	[7]
MIL-101(Cr)	77	100	3542	6.00	[8]
MIL-101(Cr)	77	60	2887	2.90	[8]
MIL-101(Cr)@AC	77	60	2998	4.40	[8]
MOF-5	77	10-20	1758	1.20	[9]
MOF-5@CNT-Pt	77	10-20	1692	1.89	[9]
HKUST-1	77	10-20	1587	2.41	[10]
HKUST-1@Li	77	10-20	795	3.50	[10]
MIL-101(Cr)	77	10-20	2537	2.37	[10]
MIL-101(Cr)@Li	77	10-20	1840	3.39	[10]
HKUST-1	77	10-20	1456	2.49	[11]
HKUST-1@Pd	77	10-20	1033	3.68	[11]

Sample	Temperature (K)	Pression (Bar)	A_{BET} (m^2 g^{-1})	Excess H_2 uptake (wt.%)	Ref.
MOF-5	77	10-20	921	1.46	[12]
MOF-5@Ni	77	10-20	802	1.53	[12]
MSC30	77	25	3305	5.6	[13]
MSP20X	77	25	2363	4.6	[13]
SA1500	77	25	2204	4.25	[13]
SA20	77	25	1737	3.1	[13]
TH90I	77	25	1204	2.9	[13]
Filtrasorb400	77	25	983	2.25	[13]

Table S5: Total hydrogen storage in gravimetric capacities (n_{tot}, wt.%) of selected MOFs reported in the literature under similar conditions (77 K, 100 bar).

Sample	Temperature (K)	Pression (Bar)	A_{BET} (m^2 g^{-1})	Total H_2 uptake (wt.%)	Ref.
NU-1500-Al	77	100	3560	8.5	[14]
NU-1501-Al	77	100	7310	14.5	[14]
NU-100	77	100	5777	14.1	[15]
SNU-70	77	100	4847	11.6	[15]
UMCM-9	77	100	4756	10.5	[15]
IRMOF-20	77	100	4127	9.5	[15]
MOF-5	77	100	3563	8.0	[15]
MOF-177	77	100	4750	9.0	[16]
C60	77	100	4750	4.5	[16]
IRMOF-20	77	100	4073	7.2	[17]
mOF-5	77	100	3512	7.5	[17]
DUT-23(Co)	77	100	5185	10.0	[17]
MOF-177	77	100	5000	10.5	[17]
MOF-177-NH2	77	100	4725	10.6	[17]
UMCM-4	77	100	4160	7.5	[17]
MIL53-Al	77	100	681	7.4	[18]
MOF-5	77	100	2589	11.5	[18]
HKUST-1	77	100	1903	9.7	[18]
MOF-177	77	100	4215	14.5	[18]
DUT-23(Co)	77	100	5117	10.7	[19]
RMOF-20	77	100	4145	9.3	[19]
MOF-5	77	100	3555	8.2	[19]

Sample	Temperature (K)	Pression (Bar)	A_{BET} ($m^2\ g^{-1}$)	Total H_2 uptake (wt.%)	Ref.
ZIF-8	77	100	1631	3.7	[19]
UIO-66	77	100	1668	7.8	[19]
Ni-MOF-74	77	100	1392	3.9	[19]
Ni-MOF-74	77	100	1736	5.4	[19]
HKUST-1	77	100	2942	8.2	[19]
UMCM-4	77	100	2931	7.8	[19]
mBr-MOF-5	77	100	2400	8.9	[19]
MSC-20	77	100	740	7.9	[19]
Norit	77	100	1740	6.4	[19]
HKUST-1	77	100	3120	10.3	[20]
NU-125	77	100	2117	6.4	[20]
rht-MOF-7	77	100	1232	3.7	[20]
Cu-MOF-74	77	100	1760	6.7	[20]
PCN-250	77	100	2460	10.8	[20]
CYCU-3-Al	77	100	2363	10.0	[20]
MSP20X	77	100	4340	12.2	[21]
NU-1101	77	100	3720	13.0	[22]
NU-1102	77	100	3305	14.9	[22]
MSC30	77	100	3560	8.5	[21]

Table S6: Total hydrogen storage in volumetric capacities (n_{tot}, kg m^{-3}) of selected MOFs reported in the literature under similar conditions (77 K, 100 bar).

Sample	Temperature (K)	Pression (Bar)	A_{BET} ($m^2\ g^{-1}$)	Total H_2 uptake (kg m^{-3})	Ref.
NU-1101	77	100	4340	41.4	[20]
NU-1102	77	100	3720	38.7	[20]
HKUST-1	77	100	1740	41.7	[20]
NU-125	77	100	3120	39.4	[20]
rht-MOF-7	77	100	2117	37.3	[20]
Cu-MOF-74	77	100	1232	36.2	[20]
PCN-250	77	100	1760	44.4	[20]
CYCU-3-Al	77	100	2460	38.1	[20]

References

[1] M.S. Amir Faiz, C.A. Che Azurahanim, S.A. Raba'ah, M.Z. Ruzniza, Low cost and green approach in the reduction of graphene oxide (GO) using palm oil leaves extract for potential in industrial applications, Results in Physics 16 (2020) 102954. https://doi.org/10.1016/j.rinp.2020.102954.

[2] S. Liu, L. Sun, F. Xu, J. Zhang, C. Jiao, F. Li, Z. Li, S. Wang, W. Ziqiang, X. Jiang, H. Zhou, L. Yang, C. Schick, Nanosized Cu-MOFs induced by graphene oxide and enhanced gas storage capacity, Energy Environ. Sci. 6 (2013) 818–823. https://doi.org/10.1039/C3EE23421E.

[3] K.P. Prasanth, P. Rallapalli, M.C. Raj, H.C. Bajaj, R.V. Jasra, Enhanced hydrogen sorption in single walled carbon nanotube incorporated MIL-101 composite metal–organic framework, International Journal of Hydrogen Energy 36 (2011) 7594–7601. https://doi.org/10.1016/j.ijhydene.2011.03.109.

[4] P.B. Somayajulu Rallapalli, M.C. Raj, D.V. Patil, K.P. Prasanth, R.S. Somani, H.C. Bajaj, Activated carbon @ MIL-101(Cr): a potential metal-organic framework composite material for hydrogen storage, International Journal of Energy Research 37 (2013) 746–753. https://doi.org/10.1002/er.1933.

[5] P.Á. Szilágyi, M. Lutz, J. Gascon, J. Juan-Alcañiz, J. van Esch, F. Kapteijn, H. Geerlings, B. Dam, R. van de Krol, MOF@MOF core–shell vs. Janus particles and the effect of strain: potential for guest sorption, separation and sequestration, CrystEngComm 15 (2013) 6003–6008. https://doi.org/10.1039/C3CE40653A.

[6] R. Balderas-Xicohténcatl, P. Schmieder, D. Denysenko, D. Volkmer, M. Hirscher, High Volumetric Hydrogen Storage Capacity using Interpenetrated Metal–Organic Frameworks, Energy Technology 6 (2018) 510–512. https://doi.org/10.1002/ente.201700608.

[7] C. Zlotea, R. Campesi, F. Cuevas, E. Leroy, P. Dibandjo, C. Volkringer, T. Loiseau, G. Férey, M. Latroche, Pd Nanoparticles Embedded into a Metal-Organic Framework: Synthesis, Structural Characteristics, and Hydrogen Sorption Properties, J. Am. Chem. Soc. 132 (2010) 2991–2997. https://doi.org/10.1021/ja9084995.

[8] Z. Yu, J. Deschamps, L. Hamon, P. Karikkethu Prabhakaran, P. Pré, Hydrogen adsorption and kinetics in MIL-101(Cr) and hybrid activated carbon-MIL-101(Cr) materials, International Journal of Hydrogen Energy 42 (2017) 8021–8031. https://doi.org/10.1016/j.ijhydene.2017.02.192.

[9] S.J. Yang, J.H. Cho, K.S. Nahm, C.R. Park, Enhanced hydrogen storage capacity of Pt-loaded CNT@MOF-5 hybrid composites, International Journal of Hydrogen Energy 35 (2010) 13062–13067. https://doi.org/10.1016/j.ijhydene.2010.04.066.

[10] Z. Xiang, Z. Hu, W. Yang, D. Cao, Lithium doping on metal-organic frameworks for enhancing H2 Storage, International Journal of Hydrogen Energy 37 (2012) 946–950. https://doi.org/10.1016/j.ijhydene.2011.03.102.

[11] X. Hu, J. Wang, S. Li, X. Hu, R. Ye, L. Zhou, P. Li, C. Chen, Pd-doped HKUST-1 MOFs for enhanced hydrogen storage: effect of hydrogen spillover, RSC Adv. 13 (2023) 14980–14990. https://doi.org/10.1039/D3RA01788E.

[12] A.M.P. Peedikakkal, I.H. Aljundi, Upgrading the Hydrogen Storage of MOF-5 by Post-Synthetic Exchange with Divalent Metal Ions, Applied Sciences 11 (2021) 11687. https://doi.org/10.3390/app112411687.

[13] P. Ramirez-Vidal, R.L.S. Canevesi, G. Sdanghi, S. Schaefer, G. Maranzana, A. Celzard, V. Fierro, A Step Forward in Understanding the Hydrogen Adsorption and Compression on Activated Carbons, ACS Appl. Mater. Interfaces 13 (2021) 12562–12574. https://doi.org/10.1021/acsami.0c22192.

[14] Z. Chen, P. Li, R. Anderson, X. Wang, X. Zhang, L. Robison, L.R. Redfern, S. Moribe, T. Islamoglu, D.A. Gómez-Gualdrón, T. Yildirim, J.F. Stoddart, O.K. Farha, Balancing volumetric and gravimetric uptake in highly porous materials for clean energy, Science 368 (2020) 297–303. https://doi.org/10.1126/science.aaz8881.

[15] A. Ahmed, S. Seth, J. Purewal, A.G. Wong-Foy, M. Veenstra, A.J. Matzger, D.J. Siegel, Exceptional hydrogen storage achieved by screening nearly half a million metal-organic frameworks, Nat Commun 10 (2019) 1568. https://doi.org/10.1038/s41467-019-09365-w.

[16] S.S. Han, J.L. Mendoza-Cortés, W.A.G. Iii, Recent advances on simulation and theory of hydrogen storage in metal–organic frameworks and covalent organic frameworks, Chem. Soc. Rev. 38 (2009) 1460–1476. https://doi.org/10.1039/B802430H.
[17] A. Ahmed, Y. Liu, J. Purewal, L.D. Tran, A.G. Wong-Foy, M. Veenstra, A.J. Matzger, D.J. Siegel, Balancing gravimetric and volumetric hydrogen density in MOFs, Energy Environ. Sci. 10 (2017) 2459–2471. https://doi.org/10.1039/C7EE02477K.
[18] P. Ramirez-Vidal, R.L.S. Canevesi, A. Celzard, V. Fierro, Modeling High-Pressure Hydrogen Uptake by Nanoporous Metal–Organic Frameworks: Implications for Hydrogen Storage and Delivery, ACS Appl. Nano Mater. 5 (2022) 759–773. https://doi.org/10.1021/acsanm.1c03493.
[19] J. Purewal, M. Veenstra, D. Tamburello, A. Ahmed, A.J. Matzger, A.G. Wong-Foy, S. Seth, Y. Liu, D.J. Siegel, Estimation of system-level hydrogen storage for metal-organic frameworks with high volumetric storage density, International Journal of Hydrogen Energy 44 (2019) 15135–15145. https://doi.org/10.1016/j.ijhydene.2019.04.082.
[20] P. García-Holley, B. Schweitzer, T. Islamoglu, Y. Liu, L. Lin, S. Rodriguez, M.H. Weston, J.T. Hupp, D.A. Gómez-Gualdrón, T. Yildirim, O.K. Farha, Benchmark Study of Hydrogen Storage in Metal–Organic Frameworks under Temperature and Pressure Swing Conditions, ACS Energy Lett. 3 (2018) 748–754. https://doi.org/10.1021/acsenergylett.8b00154.
[21] G. Sdanghi, S. Schaefer, G. Maranzana, A. Celzard, V. Fierro, Application of the modified Dubinin-Astakhov equation for a better understanding of high-pressure hydrogen adsorption on activated carbons, International Journal of Hydrogen Energy 45 (2020) 25912–25926. https://doi.org/10.1016/j.ijhydene.2019.09.240.
[22] D.A. Gómez-Gualdrón, T.C. Wang, P. García-Holley, R.M. Sawelewa, E. Argueta, R.Q. Snurr, J.T. Hupp, T. Yildirim, O.K. Farha, Understanding Volumetric and Gravimetric Hydrogen Adsorption Trade-off in Metal–Organic Frameworks, ACS Appl. Mater. Interfaces 9 (2017) 33419–33428. https://doi.org/10.1021/acsami.7b01190.